Arabian Journal of Chemistry (2019) **12**, 1406–1412

King Saud University

Arabian Journal of Chemistry

www.ksu.edu.sa
www.sciencedirect.com

ORIGINAL ARTICLE

Photodegradation of rhodamine B over semiconductor supported gold nanoparticles: The effect of semiconductor support identity

Ahmad Alshammari *, **Abdulaziz Bagabas, Muhamad Assulami**

Materials Science Research Institute (MSRI), King Abdulaziz City for Science and Technology (KACST), P.O. Box 6086, Riyadh 11442, Saudi Arabia

Received 28 July 2014; accepted 3 November 2014
Available online 10 November 2014

KEYWORDS

Supported AuNPs;
Semiconductor photocatalyst;
Photodegradation;
Rhodamine B

Abstract Rhodamine B (RB) is a toxic dye used extensively in textile industry, which must be remediated before its drainage to environment. In the present study, supported gold nanoparticles on commercially available titania and zincite were successfully prepared and then their activity on the photodegradation of RB under UV A light irradiation was evaluated. The synthesized photocatalysts were characterized by ICP, BET, XRD, TEM and EDX. Kinetic results showed that Au/TiO_2 was a photocatalyst inferior to Au/ZnO. This observation could be attributed to the strong reflection of UV irradiation by gold nanoparticles over TiO_2 support.

1. Introduction

Securing suitable water for drinking and irrigation purposes is an important issue across the globe. Water purification and recycling, in addition, is a preventive measurement of environment contamination and a saving tool of water in arid places. Industries contribute significantly to environment pollution by various ways such as wastewater effluent (Singh et al., 2007; Lilja and Liukkonen, 2008; Garcíaa et al., 2008, 2013; Dermeche et al., 2013; Ahmed et al., 2011). Textile industries, for instance, contaminate water by draining aqueous dye pollutant solutions (Mahmoodi et al., 2007; Neumann et al., 2002). Adsorption is a good treatment technique for the abatement of dye wastewater stream (Visvanathan and Asano, 2009). However, this technique generates waste solid, which requires further purification of the adsorbent materials and treatment of the separated pollutant. Therefore, such a procedure increases the cost of water purification, but it would help us avoid landfill with solid wastes. Furthermore, depending on the nature of the adsorbent material, regeneration process may produce the adsorbent with its same original activity or less. The adsorbent may lose its activity after a certain number of recycling. Thus, with all these drawbacks of adsorption technique, advanced heterogeneous photocatalytic oxidation of dye pollutants emerges as an effective, economic alternative technique because of the complete destruction of the dye

* Corresponding author. Fax: +966 11 481 4574.
E-mail address: aalshammari@kacst.edu.sa (A. Alshammari).
Peer review under responsibility of King Saud University.

Production and hosting by Elsevier

http://dx.doi.org/10.1016/j.arabjc.2014.11.013
1878-5352

pollutant by the generated active oxygen-containing species under the illumination of UV–visible light to much less harmful products and with the ease of photocatalyst separation and recyclability (Gupta et al., 2000; Rajeshwar et al., 1994; Rahimi et al., 2012; Aliabadi and Sagharigar, 2011; Bagabas et al., 2010; Libanori et al., 2009; Wilhelm and Stephan, 2007; Silva et al., 2014).

Semiconductors have been widely used as photocatalysts in advanced photocatalytic oxidation technique. Depending on the band gap energy (E_g) of the semiconductor photocatalyst, either UV or Visible irradiation can be used for excitation and generation of exciton (electron–hole pair), needed for redox decomposition of pollutant. Titania, TiO_2, and zincite, ZnO, have a wide E_g of ~3.2 eV (Reddy et al., 2002; Monllor-Satoca et al., 2007; Welte et al., 2008), making them appropriate absorbents of long wave ultraviolet light (UV A, 3.1–3.94 eV) (Gupta et al., 2000; Rajeshwar et al., 1994; Rahimi et al., 2012; Aliabadi and Sagharigar, 2011). However, their E_g is tunable by doping them with other semiconductor or metal nanoparticles. The doping process enhances their photocatalytic performance through charge separation and minimization or elimination of electron–hole recombination (Rahimi et al., 2012; Libanori et al., 2009; Silva et al., 2014; Yu et al., 2013). Metal nanoparticles such as gold act as electron drain or electron donar whether the excitation is made by UV or visible irradiation (Silva et al., 2014; Yu et al., 2013).

Several studies have focused on promoting the photocatalytic performance of TiO_2 and ZnO by doping with gold nanoparticles (AuNPs) (e.g., Silva et al., 2014; Yu et al., 2013). However, there are a few or no studies comparing these two semiconductor supports and exploring their effect on AuNPs. Therefore, in this work we have tried to find out the effect of TiO_2 and ZnO supports promoted with AuNPs on the photodegradation of rhodamine B (RB) in aqueous medium, under UV A light irradiation.

2. Material and methods

2.1. Materials

Tetrachloroauric acid trihydrate ($HAuCl_4{\cdot}3H_2O$, ⩾99.9% trace metal basis, Sigma–Aldrich), sodium citrate dihydrate (⩾99%, FG, Aldrich), tannic acid (ACS reagent, Sigma–Aldrich), rhodamine B (⩾95% HPLC, Sigma), titanium dioxide (purum, >99%, Fluka), and zinc oxide (99%, ACS reagent, Riedel-De Haen AG) were commercially available and were used without further purification. Deionized water (18.2 MΩ cm) was obtained from a Milli-Q water purification system (Millipore).

2.2. Synthesis of photocatalyst

Catalysts were prepared in two steps using the commercially available TiO_2 and ZnO as oxidic supports. The first step dealt with the preparation of the colloidal AuNPs by the reduction of $HAuCl_4$ in aqueous solution using 1 wt.% tannic acid and 1 wt.% sodium citrate. The second step involved the impregnation of the colloidal AuNPs with an oxidic support to obtain slurry, which was stirred for 2 h at room temperature and then the excess solvent was removed by a rotary evaporator. The obtained solids were oven-dried at 120 °C for 16 h and then were calcined at 350 °C for 5 h in air. The loading of AuNPs was fixed at 1 wt.%. More details on the catalyst preparation are described elsewhere (Alshammari et al., 2012).

2.3. Characterization

Au-content was determined by inductively-coupled plasma optical emission spectroscopy (ICP-OES). BET specific surface areas were estimated by nitrogen physisorption method at −196 °C. X-ray diffraction (XRD) patterns were recorded for phase analysis on a Philips X pert pro diffractometer, operated at 40 mA and 40 kV by using CuK_α radiation and a nickel filter, in the 2-theta range from 2° to 80° in steps of 0.02°, with a sampling time of one second per step. Morphology of the catalyst was explored by transmission electron microscopy (TEM, JEM-2100F JEOL). Carbon-coated copper grids were used for mounting the samples for TEM analysis. TEM was equipped with EDX for element analysis. Solid-state ultraviolet–visible (UV–Vis) absorption and reflectance spectra for photocatalyst powder samples were recorded on a Perkin Elmer Lambda 950 UV/Vis/NIR spectrophotometer, equipped with a 150 mm snap-in integrating sphere for capturing diffuse and specular reflectance.

2.4. Photocatalytic test

Photocatalytic experiments were carried out in a glass beaker containing 100 ml of 20 mg L^{-1} RB solution and 100 mg of photocatalyst sample, using Luzchem Photoreactor. Before exposure to UV A light irradiation, the reaction mixture was magnetically stirred in the dark for 1 h to ensure adsorption/desorption equilibrium of the dye on the photocatalyst surface. Afterwards, the reaction suspension was irradiated by 365-nm UV light at a power of 54.3 W/m^2. Aliquot samples taken from the reaction mixture at every 20-min interval, were centrifuged for photocatalyst separation, and then absorbance was recorded at λ_{max} of 554 nm using the UV/Vis/NIR spectrophotometer. The RB dye concentration of the samples was estimated using established calibration curve. The percentage of degradation of dye was measured by applying the following equation: % Degradation = $(C_0 - C)/C_0 \times 100$, where C_0 is the initial concentration of RB dye and C is the equilibrium concentration of RB dye after irradiation.

3. Results and discussion

3.1. Chemical composition and N_2-physisorption

ICP results (Table 1) showed that the loading of AuNPs on ZnO and TiO_2 is in line with the nominal content of Au (1 wt.%). Table 1 displays also the BET specific surface areas and pore volumes of AuNPs supported on ZnO and TiO_2. The

Table 1 ICP and BET surface area results of AuNPs over ZnO and TiO_2.

Catalyst	ICP (wt.%)	BET surface area (m^2/g)		Pore volume (cm^3/g)
		Undoped	Au-doped	
Au/ZnO	0.9	45	39	0.10
Au/TiO_2	0.9	47	43	0.12

Undoped sample indicates support only.

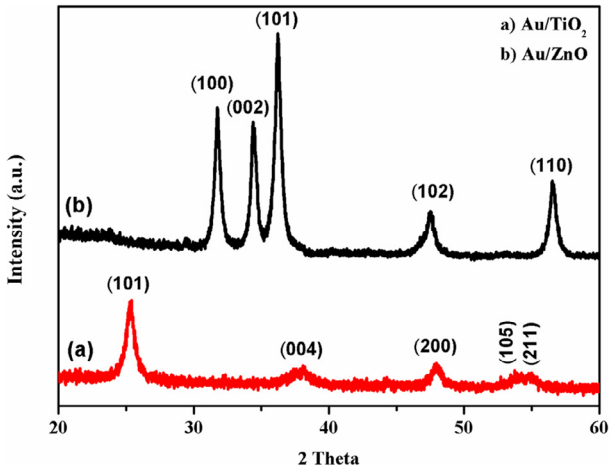

Figure 1 XRD patterns of AuNPs supported on (a) TiO_2 and (b) ZnO.

Au/TiO_2 photocatalyst has a slightly higher BET surface area than the Au/ZnO photocatalyst, whereas undoped ZnO and TiO_2 have similar surface areas. The surface area of supports decreased after impregnation with AuNPs. These results indicate that the AuNPs are highly dispersed on the support without any sintering effect. Such good dispersion is also confirmed by XRD and TEM, as shown later.

3.2. XRD phase identification

XRD patterns of AuNPs supported on ZnO and TiO_2 are displayed in Fig. 1. The XRD pattern of Au/TiO_2 showed the presence of anatase phase, as verified by the appearance of diffraction peaks at 2θ values of 25.4°, 37.9°, 48.1°, 54.0°, and 55.2° corresponding to (101), (004), (200), (105), and (211) crystallographic planes of anatase, respectively. Diffraction peaks located at 2θ values of 31.84°, 34.52°, 36.33°, 47.63°, 56.71°, 62.96°, 68.13°, and 69.18° correspond to (100), (002), (101), (102), and (110) crystallographic planes of ZnO hexagonal wurtzite phase. In addition, Fig. 1 reveals that no diffraction peaks corresponding to metallic Au can be observed in Au/ZnO and Au/TiO_2. Such observation could be due to their high dispersion and their small size, lending good support to the observed size of AuNPs by TEM ($\leqslant$5 nm). On the other hand, the XRD pattern reveals diffraction peaks corresponding to the supports only.

3.3. Size and morphology of Au/TiO_2 and Au/ZnO

Representative TEM images of AuNPs supported on TiO_2 and ZnO are shown in Fig. 2a and b. AuNPs are almost spherical and dispersed on the supports, while their particle size depends strongly on the nature of support. As shown in the inset of Fig. 2a and b, Au/TiO_2 and Au/ZnO resulted in a narrow particle size distribution in the range from 1 to 3 nm and 1 to 5, respectively. In addition, (HR)-TEM image (shown as insert in Fig. 2) enabled the observation of the crystal planes of AuNPs. The lattice d-spacing measured using HRTEM for Au/TiO_2 and Au/ZnO is presented as inset images in Fig. 2a and b, respectively, and were compared with those of bulk Au (Table 2). This figure illustrates HRTEM and corresponding

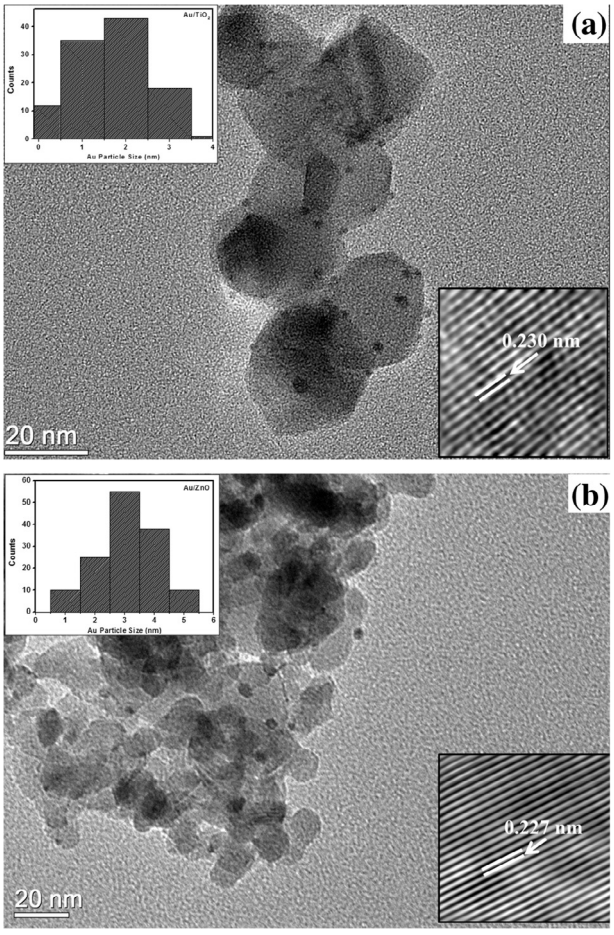

Figure 2 TEM images of AuNPs supported on (a) TiO_2 and (b) ZnO. Inset images show crystal planes of AuNPs in Au/TiO_2 (in set a) and Au/ZnO (in set b). Histogram showing particle size of AuNPs supported on (inset a) TiO_2 and (inset a) ZnO.

fast Fourier transform (FFT) and clearly shows that the inter planar spacing is visible and the gold particles are crystallized with an inter-planar spacing of approximately 0.230 nm for Au/TiO_2 and 0.227 for Au/ZnO. According to JCPDS No. 4-784 and the Bragg diffraction law, these values are very close to the bulk 0.235 nm d-spacing for the (111) plane in the face-centered cubic (fcc) phase of gold (Wong-Ng et al., 2001).

3.4. Element composition and EDX mapping

The element composition on the surface of Au/TiO_2 and Au/ZnO photocatalysts is further confirmed by dispersive X-ray (EDX) spectroscopy analysis. As shown in Fig. 3a and b, EDX results for the Au/TiO_2 and Au/ZnO confirmed that

Table 2 Inter planar spacing and diffraction planes of AuNPs supported on TiO_2 and ZnO carriers.

Sample	d-Spacing calculated from HRTEM, (nm)	d-Spacing in bulk Au, (nm)	Miller indices (hkl) assignment
Au/TiO_2	0.230	0.235	111
Au/ZnO	0.227	0.235	111

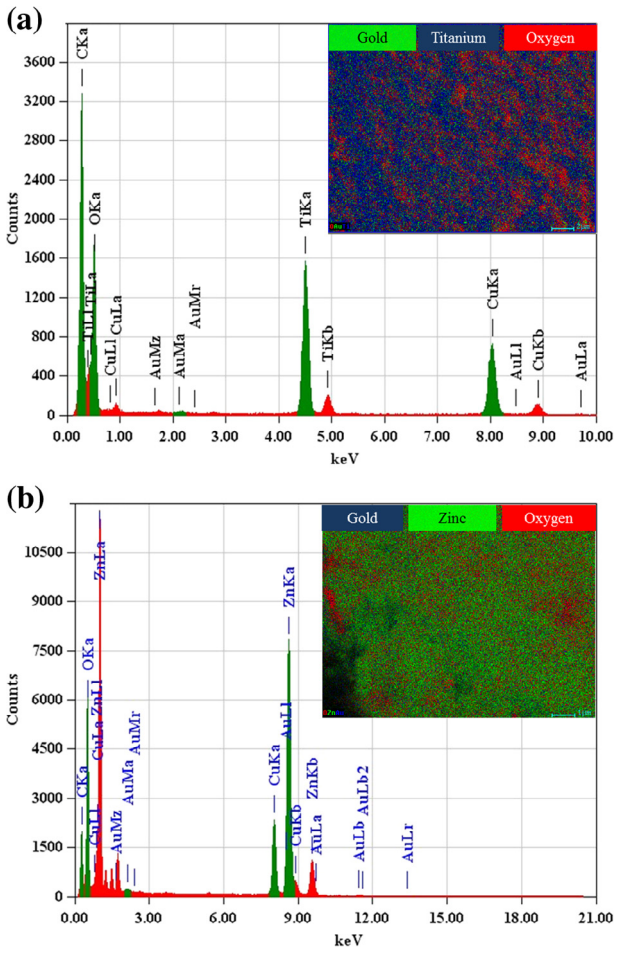

Figure 3 Element composition and EDX mapping (inset) of AuNPs supported on (a) TiO_2 and (b) ZnO.

the surface of these catalysts was composed of the expected elements (Au, Ti or Zn (intense signals), and O). The Cu and C peaks are ascribed to the carbon-coated Cu grid used as a sample holder. EDX mapping was also carried out to explore more information about the elemental constituents and distribution pattern of Au nanoparticles on the surface of TiO_2 and ZnO (as shown in the inset of Fig. 3a and b). Fig. 3a obviously presents the distribution of Au (green dots), Ti (blue dots) and O (red dots) for 1% of AuNPs supported on TiO_2. It is observed from this figure that Ti is distributed virtually uniformly throughout the bulk surface, whereas Au, despite its low loading, is homogeneously present with clusters on some spots of the surface. However, O is not distributed evenly on the surface. On the other hand, mapping of the element composition of the surface nanostructure of 1% AuNPs supported on ZnO showed that Zn (green dots) is the most scattered element and the most abundant element on the surface, while Au (blue dots) has a low concentration on surface and O (red dots) has a higher concentration than Au and lower than that of Zn. Results (EDX and mapping) in Fig. 3a and b revealed that the concentration of Zn on the surface of Au/ZnO was higher than the concentration of Ti on Au/TiO_2 catalyst. Since the metal sites represent Lewis acidic sites, we might expect that Au/ZnO photocatalyst exhibits higher photocatalytic performance than Au/TiO_2 photocatalyst. This expectation is based on the one previously reported for the importance of surface acidity and its role in enhancing photocatalytic activity (Papp et al., 1994).

3.5. Solid-state UV–vis spectrophotometry

Fig. 4a and b exhibits UV–vis absorption spectra of the undoped supports (ZnO and TiO_2) and the AuNPs-supported photocatalysts (Au/ZnO and Au/TiO_2). The broad surface plasmon resonance (SPR) band between 500 and 750 nm is due to the presence of AuNPs on the ZnO and TiO_2 surfaces, as confirmed by XRD and TEM results. In contrast, the absorbance from 200 to 390 nm is due to ZnO or TiO_2. The position and shape of SPR depends on different factors such as particle size, shape, and dielectric constant of the medium [Mie, 1908; Ozbay, 2006]. The indirect band gap (E_g) estimation from these spectra for the undoped TiO_2 support and the AuNPs-supported on TiO_2 (Au/TiO_2) is illustrated in Fig. 4c, where the x-axis represents the photon energy (E) in eV and the y-axis represents the square root of the product of absorption coefficient (α) and energy $(E\alpha)^{0.5}$. The direct band gap (E_g) estimation from these spectra for the undoped ZnO support and the AuNPs-supported on ZnO (Au/ZnO) is illustrated in Fig. 4d, where the x-axis represents the photon energy (E) in eV and y-axis represents the square of the product of absorption coefficient (α) and energy $(E\alpha)^2$. The E_g for undoped ZnO and TiO_2 were 3.27 and 2.90 eV, respectively. The indirect band gap value of TiO_2 was reduced to 2.51 eV after Au loading, while a slight decrease to 3.23 eV was observed in the direct band gap of Au/ZnO. Such observation implies that the optical properties of these materials are affected by the nature of the support. The reduction in the band gap of TiO_2 after loading AuNPs could be attributed to the "strong metal-support interaction, SMSI" because TiO_2 is a well-known material exhibiting such phenomenon (Tauster, 1987). This conclusion regarding the reduction of band gap due to SMSI could be supported by the higher absorption intensity of Au/TiO_2 in the visible light region in comparison to Au/ZnO (as shown in Fig. 4a and b). The increase in absorption intensity upon Au loading over TiO_2 and ZnO implies higher photocatalytic activity under UV and visible light irradiation (Yu et al., 2013).

Fig. 5 shows the UV–visible reflectance spectra of both Au/TiO_2 and Au/ZnO photocatalysts in the range of 200–800 nm. Au/TiO_2 photocatalyst has a higher reflectance percentage (R%) than Au/ZnO photocatalyst in the UV range from 226 nm to 382 nm, as shown in the inset of Fig. 5. Due to this fact, less UV A photons are absorbed by Au/TiO_2 photocatalyst, and hence, less excitons are generated and less photocatalytic activity are observed. In addition, the lesser reflectance percentage of Au/TiO_2 in the visible region as compared to Au/ZnO (as shown in Fig. 5) can also give another hint for the SMSI effect on the band gap of Au/TiO_2.

3.6. Photocatalytic degradation of RB

Fig. 6 exhibits the UV–vis absorption spectra of a 20 mg L^{-1} Rhodamine B solution before and after UV A light irradiation in a time interval of 20 min in the presence of (a) Au/TiO_2 and (b) Au/ZnO as photocatalysts. Prior to irradiation with UV A light, an experiment was carried out in the dark to ensure whether adsorption of dye occurred on the surface of catalyst

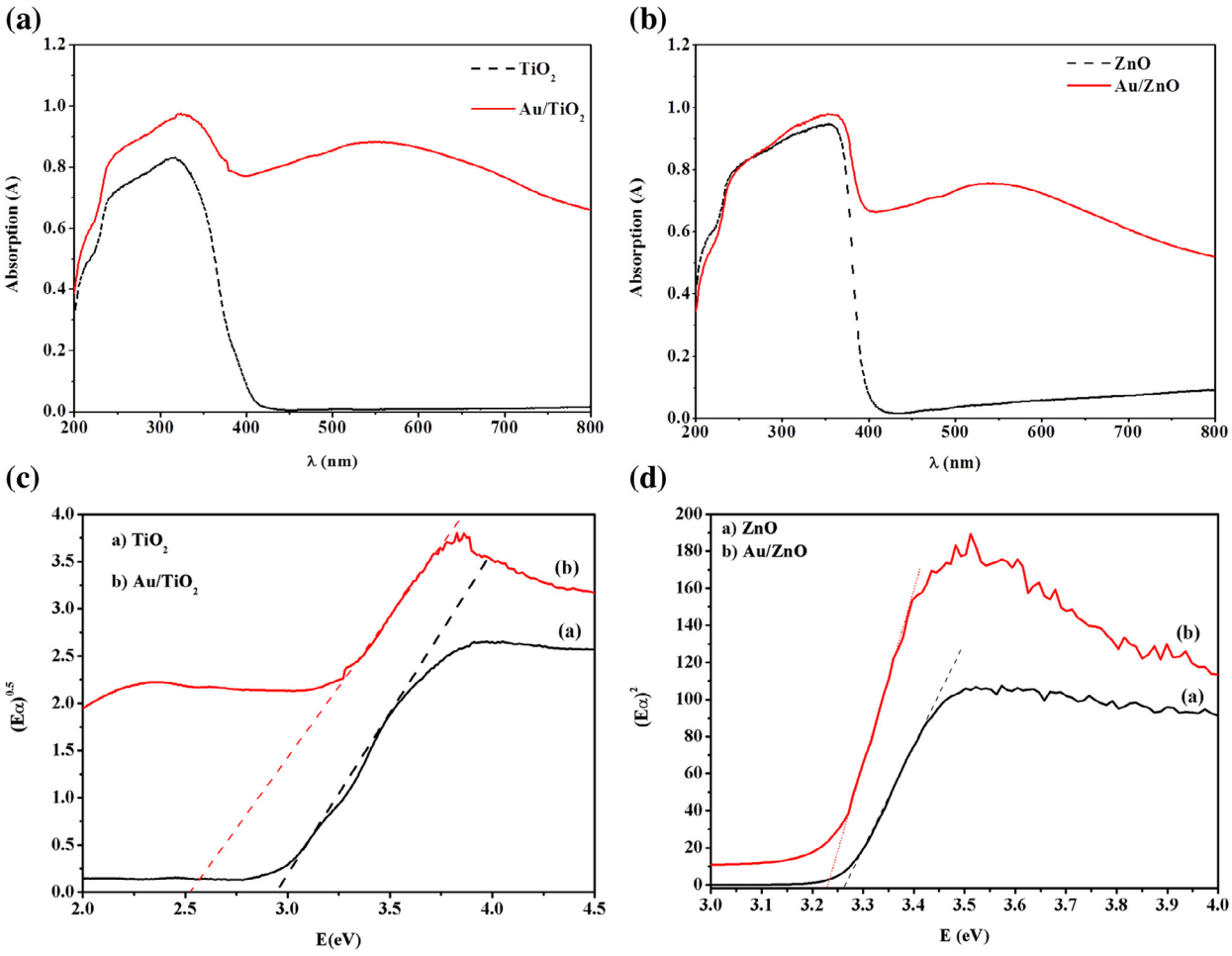

Figure 4 UV–vis absorption spectrum for AuNPs supported on (a) TiO_2 and (b) ZnO and direct band-gap for AuNPs supported on (c) TiO_2 and (d) ZnO, respectively.

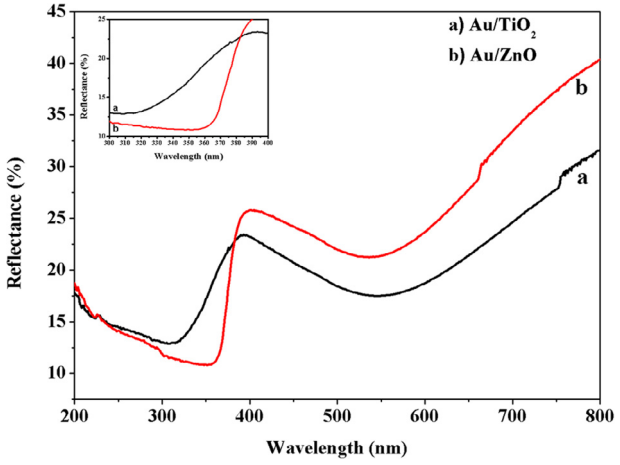

Figure 5 UV–visible reflectance spectra of both Au/TiO_2 and Au/ZnO.

or not. This experiment confirmed that a slight decrease in concentration of RB was observed due to adsorption and found to be comparable for both Au/TiO_2 and Au/ZnO photocatalysts. According to Fig. 6a, the absorption peaks at 554 nm decreased with increasing irradiation time and finally vanished after 100 min of UV irradiation. In the case of Au/ZnO photocatalyst (Fig. 6b), the characteristic absorption band of RB at 554 nm decreased significantly with increasing irradiation time without appearance of other absorption features. It can be seen from Fig. 4b that the absorbance of RB almost disappeared after 80 min. As compared with the absorbance of RB with Au/ZnO, the photocatalytic activity of Au/TiO_2 showed a slower degradation which reached zero after 100 min. These results indicate that Au over ZnO has better photocatalytic activity than Au over TiO_2.

Furthermore, we found that the photocatalytic degradation of RB in aqueous medium using undoped and Au-doped photocatalysts depended on the identity of the support, as evidenced by the degradation plot in Fig. 7. The RB photodegradation reactions over either undoped TiO_2 or undoped ZnO are similar in the first 60 min with degrading ~73% of the present RB dye in solution. However, TiO_2 performance afterward became better than that of ZnO until 160 min of the reaction time. The RB degradation of ~98% efficiency was achieved over either TiO_2 or ZnO at 160 min of reaction and the degradation efficiency was constant afterward with increasing reaction time. The stability of photocatalytic performance at and beyond 160 min could be attributed to the accumulation of the degradation products on the surface of the photocatalyst. On the other hand, doping both of

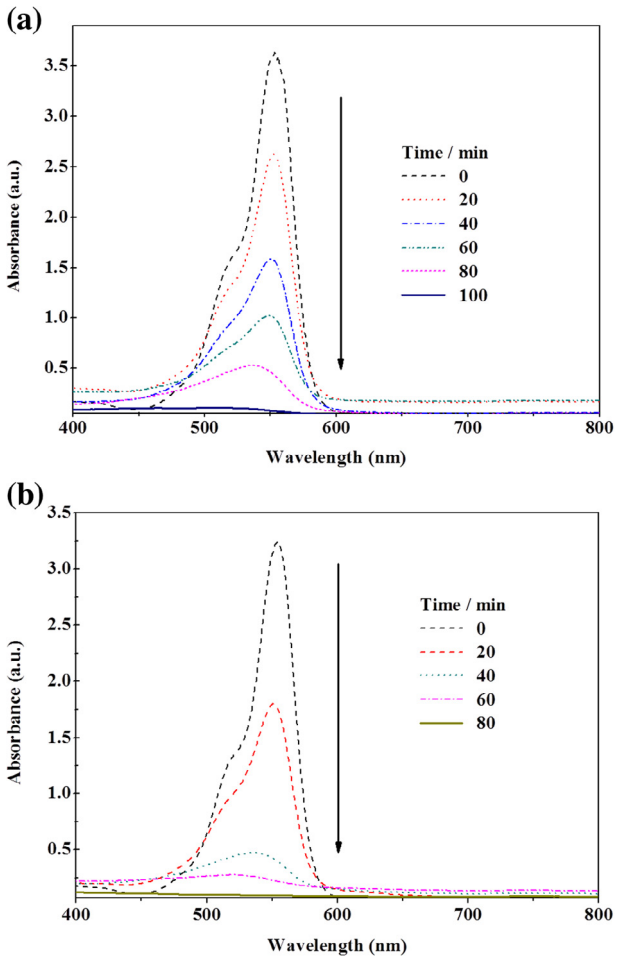

Figure 6 Absorption spectra of RB at different times after UV irradiation using (a) Au/TiO_2 and (b) Au/ZnO as photocatalysts.

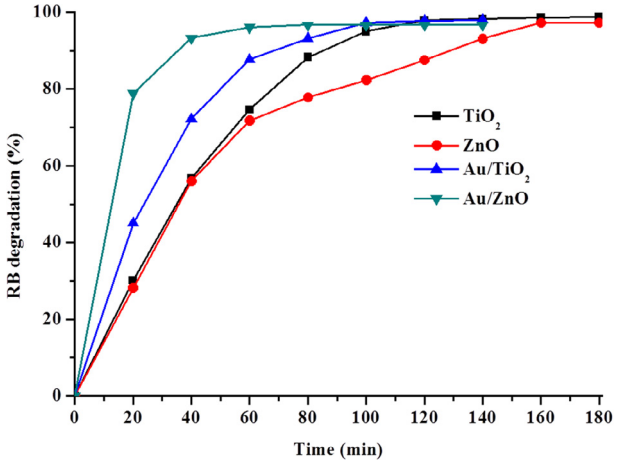

Figure 7 Photocatalytic degradation of RB under UV irradiation catalyzed with TiO_2 ZnO, Au/TiO_2 and Au/ZnO.

TiO_2 and ZnO with 1 wt.% AuNPs resulted in enhancing the RB photodegradation performance. The Au/TiO_2 photocatalyst resulted in 87% degradation efficiency after 60 min of the reaction while the Au/ZnO photocatalyst caused 96% degradation efficiency after 60 min. The enhancement in the

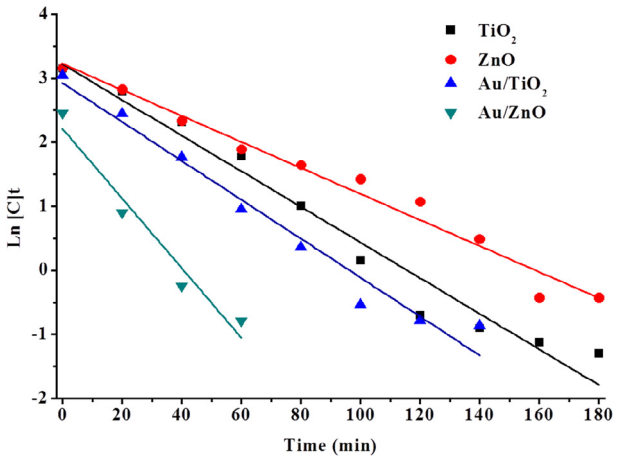

Figure 8 Kinetic data for the degradation of RB under UV irradiation catalyzed with TiO_2 ZnO, Au/TiO_2 and Au/ZnO.

photocatalytic degrading capability of both TiO_2 and ZnO could be attributed to the electron buffering of AuNPs, which in turn impede the recombination of electron–hole pairs (Yu et al., 2013). However, the lower performance of Au/TiO_2 than Au/ZnO could be due to the strong reflection of UV irradiation by AuNPs over TiO_2 support, as shown previously in Fig. 5 in Section 3.5. With an increasing reaction time to 80 min, the degradation efficiency of Au/ZnO photocatalyst increased very slightly to 97% and stabilized at this value with the progress of reaction. On the other hand, the photocatalytic degradation capability of Au/TiO_2 gradually increased to 97% upon increasing reaction time from 60 min to 100 min, after which efficiency was maintained at this value. The plateau region of photocatalysts suggests the occurrence of deactivation by deposition of the reaction products on the photocatalyst surface.

3.7. Kinetics of photodegradation of RB

The pseudo first order kinetic photodegradation of RB was estimated by the following mathematical expression:

$$\mathrm{Ln}[C]_t = -k_{app}t + \mathrm{Ln}[C]_0$$

where $[C]_0$ and $[C]_t$ are the concentrations of RB in solution (in unit of mg L^{-1}) at time zero and at time (t) of illumination, respectively, and (k_{app}) is the apparent rate constant (min^{-1}). The kinetic analysis of RB photodegradation is illustrated in Fig. 8, which shows that the catalyst identity affects strongly the rate of photocatalytic reaction. Table 3 displays k_{app} and the half-life ($t_{1/2}$) of the pseudo first-order RB photodegradation reaction. The reaction proceeds ~1.4 faster over undoped TiO_2 than undoped ZnO. However, doping TiO_2 with Au

Table 3 k_{app} and half-life ($t_{1/2}$) of the pseudo first-order RB photodegradation reaction.

Photocatalyst	k_{app} (min^{-1})	$t_{1/2}$ (min)
TiO_2	2.78×10^{-2}	24.93
ZnO	2.03×10^{-2}	34.14
Au/TiO_2	3.04×10^{-2}	22.80
Au/ZnO	5.44×10^{-2}	12.74

slightly speeded up the reaction by a factor of 1.1 in comparison to undoped TiO_2, while doping ZnO with Au increased the reaction rate by a factor of ~2.7 in comparison to undoped ZnO. These kinetic parameters reflect how the support and its interaction with AuNPs influence the catalytic performance.

4. Conclusion

Supported gold nanoparticles on commercially available titania and zincite were successfully synthesized and then their activity on the photodegradation of RB under UV A light irradiation was evaluated. Photocatalytic results showed that doping titania and zincite with 1 wt.% AuNPs accelerated the RB photodegradation over zincite and made it ~2.7 times faster than that of undoped zincite, ~2.0 times that of undoped titania, and ~1.8 times that of titania supported AuNPs. The lower performance of titania supported AuNPs than zincite supported gold nanoparticles is due to the strong reflection of UV irradiation by gold nanoparticles over titania support. These findings explicitly reflect the key role of semiconductor support in the photocatalytic degradation of RB dye under UV A light irradiation.

Acknowledgments

This study was supported by King Abdulaziz City for Science and Technology (KACST) through project No. 29-280. We also thank Mr. Abdulaziz Arromaih for TEM analysis.

References

Ahmed, S., Rasul, M.G., Brown, R., Hashib, M.A., 2011. Influence of parameters on the heterogeneous photocatalytic degradation of pesticides and phenolic contaminants in wastewater: a short review. J. Environ. Manage. 92, 311–330.

Aliabadi, M., Sagharigar, T., 2011. Photocatalytic removal of rhodamine B from aqueous solutions using TiO_2 nanocatalyst. J. Appl. Environ. Biol. Sci. 1, 620–626.

Alshammari, A., Koeckritz, A., Kalevaru, V.N., Bagabas, A., Martin, A., 2012. Significant formation of adipic acid by direct oxidation of cyclohexane using supported nano-gold catalysts. ChemCatChem 4, 1330–1336.

Bagabas, A., Gondal, M., Dastageer, A., Yamani, Z., Ashameri, M., 2010. Laser-induced photocatalytic inactivation of coliform bacteria from water using pd-loaded nano-WO_3. Stud. Surf. Sci. Catal. 175, 279–282.

Dermeche, S.M., Nadour, C., Larroche, Moulti-Mati, F., Michau, P., 2013. Olive mill wastes: biochemical characterizations and valorization strategies. Process Biochem. 48, 1532–1552.

Garcíaa, V., Pongracz, E., Phillips, P., Keiski, R.L., 2008. Factors affecting resource use optimisation of the chemical industry in the Northern Ostrobothnia region of Finland. J. Clean. Prod. 16, 1987–1994.

Garcíaa, V., Pongrácza, E., Phillips, P.S., Keiski, R.L., 2013. From waste treatment to resource efficiency in the chemical industry: recovery of organic solvents from waters containing electrolytes by pervaporation. J. Clean. Prod. 39, 146–153.

Gupta, V.K., Mohan, D., Sharma, S., Sharma, M., 2000. Removal of basic dyes (rhodamine B and methylene blue) from aqueous solutions using bagasse fly ash. Sep. Sci. Technol. 35, 2097–2113.

Libanori, R., Giraldi, T.R., Longo, E., Leite, E.R., Ribeiro, C., 2009. Effect of TiO_2 surface modification in Rhodamine B photodegradation. J. Sol-Gel Sci. Tech. 49, 95–100.

Lilja, R., Liukkonen, S., 2008. Industrial hazardous wastes in Finland – trends related to the waste prevention goal. J. Clean. Prod. 16, 343–349.

Mahmoodi, N.M., Armani, M., Lymaee, N.Y., Gharanjig, K., 2007. Photocatalytic degradation of agricultural N-heterocyclic organic pollutants using immobilized nanoparticles of titania. J. Hazard. Mater. 145, 65–71.

Mie, G., 1908. A contribution to the optics of turbid media, especially colloidal metallic suspensions. Ann. Phys. 25, 377–445.

Monllor-Satoca, D., Gomez, R., González-Hidalgo, M., Salvador, P., 2007. The "Direct–Indirect" model: an alternative kinetic approach in heterogeneous photocatalysis based on the degree of interaction of dissolved pollutant species with the semiconductor surface. Catal. Today 129, 247–255.

Neumann, M., Schulz, R., Schäfer, K., Müller, W., Mannheller, W., Liess, M., 2002. The significance of entry routes as point and non-point sources of pesticides in small streams. Water Res. 36, 835–842.

Ozbay, E., 2006. Plasmonics: merging photonics and electronics at nanoscale dimensions. Science 331, 189–193.

Papp, J., Soled, S., Dwight, K., Wold, A., 1994. Surface acidify and photocatalytic activity of TiO_2, WO_3/TiO_2, and MoO_3/TiO_2 photocatalysts. Chem. Mater. 6, 496–500.

Rahimi, R., Bathaee, H., Rabbani, M., Degradation of Rhodamine B Using Cr-doped TiO_2 under Visible Light Irradiation. 16th Intern. Electronic Conference on Synthetic Organic Chem. (ECSOC-16), 1st November, 2012.

Rajeshwar, K., Ibanez, J.G., Swain, G.M., 1994. Electrochemistry and the environment. J. Appl. Electrochem. 24, 1077–1091.

Reddy, K., Manorama, S., Redd, A., 2002. Band gap studies on anatase titanium dioxide nanoparticles. Mater. Chem. Phys. 78, 239–245.

Silva, C.G., Sampaio, M.J., Carabineiro, S., Oliveira, J., Baptista, D.L., Bacsa, R., Machado, B.F., Serp, P., Figueiredo, J.L., Silva, A., Faria, J.L., 2014. Developing highly active photocatalysts: gold-loaded ZnO for solar phenol oxidation. J. Catal. 316, 182–190.

Singh, I.B., Chaturvedi, K.R., Morchhale, K.A., Yegneswaran, H., 2007. Thermal treatment of toxic metals of industrial hazardous wastes with fly ash and clay. J. Hazard. Mater. 141, 215–222.

Tauster, S.J., 1987. Strong metal-support interactions. Acc. Chem. Res. 20, 389–394.

Visvanathan, C., Asano, T., 2009. The potential for industrial wastewater reuse. In: Vigneswaran, S. (Ed.), Wastewater Recycle, Reuse, and Reclamation. EOLSS, e-book, pp. 299–317.

Welte, A., Waldauf, C., Brabec, C., Wellmann, P., 2008. Application of optical for the investigation of electronic and structural properties of sol-gel processed TiO_2 films. Thin Solid Films 516, 7256–7259.

Wilhelm, P., Stephan, D., 2007. Photodegradation of rhodamine B in aqueous solution via $SiO_2@TiO_2$ nano-spheres. J. Photochem. Photobiol., A: Chem. A 185, 19–25.

Wong-Ng, W., McMurdie, H.F., Hubbard, C.R., Mighell, A.D., 2001. JCPDS-ICDD research associateship (cooperative pro-gram with NBS/NIST). J. Res. Natl. Inst. Stand Technol. 106, 1013–1028.

Yu, H., Ming, H., Gong, J., Li, H., Huang, H., Pan, K., Liu, Y., Kang, Z., Wei, J., Wang, D., 2013. Facile synthesis of Au/ZnO nanoparticles and their enhanced photocatalytic activity for hydroxylation of benzene. Bull. Mater. Sci. 36, 367–372.